Fe^{II} Bi-Stable Materials Based on Dissymmetrical Ligands: N_4 Schiff Bases Including 2-Pyridyl and 5-Methylimidazol-4-yl Rings Yield Various Fe^{II} Spin-Crossover Phenomena around 300 K

Nicolas Bréfuel,[†] Sergiu Shova,[†,‡] Janusz Lipkowski,[§] and Jean-Pierre Tuchagues*[,†]

Laboratoire de Chimie de Coordination du CNRS, UPR 8241, 205 route de Narbonne, 31077 Toulouse cedex 04, France, and Institute of Physical Chemistry, Polish Academy of Sciences, Kasparzaka 44/52, PL-01 224 Warszawa, Poland

Received July 1, 2006. Revised Manuscript Received August 30, 2006

The synthesis and characterization of six new spin-crossover (SCO) materials $[FeL^{Dx}(NCX)_2]$ (**1**: X = S, $x = 1$; **2**: X = Se, $x = 1$; **3**: X = S, $x = 2$; **4**: X = Se, $x = 2$; **5**: X = S, $x = 3$; **6**: X = S, $x = 4$) are reported, where $L^{D1}-L^{D4}$ stand for the dissymmetrical tetradentate ligands obtained by 1:1:1 Schiff base condensation of 1,3-diaminopropane (L^{D1}, L^{D3}) or 2,2-dimethyl-1,3-diaminopropane (L^{D2}, L^{D4}), 2-acetylpyridine (L^{D1}, L^{D2}) or 6-bromo-2-acetylpyridine (L^{D3}, L^{D4}), and 5-methylimidazole-4-carboxaldehyde. Magnetic and Mössbauer studies and X-ray structures at 100, 200, and 300 K (low-spin (LS) state) and 350 and 400 K (high-spin (HS) state) for **3**, and 180 K (HS state) for **6** revealed the occurrence of unusual SCO behaviors: complex **3** undergoes a first-order SCO centered at 315 K with a 4 K wide hysteresis associated with an order−disorder phenomenon for the propylene fragment of L^{D2}, whereas **1** exhibits a two-step SCO occurring at ∼202 (smooth) and 297.5 K (11 K wide hysteresis). A significant mass effect is induced upon changing the thiocyanate for selenocyanate ligands: the SCO of **4** (NCSe) occurs ∼100 K higher than for **3**. These new features are discussed comparatively to the results obtained for a related series of SCO materials. **5** and **6**, which include a 6-bromopyridyl substituent, remain HS over the whole 80−300 K range.

Introduction

Octahedral Fe^{II} complexes that undergo a thermal spin-crossover (SCO) are a well-known form of molecular switch in which a change in the electronic configuration of the metal center (low-spin (LS), $S = 0$, $^1A_1$ ↔ high-spin (HS), $S = 2$, $^5T_{2g}$) usually leads to drastic changes in the molecular geometry, color, and magnetic properties.[1] The main requirement for a possible use of SCO materials as active elements in memory devices is the occurrence of a steep SCO with a relatively large thermal hysteresis centered at ambient temperature.[2] Cooperative effects, resulting from intermolecular interactions, are the key to such a magnetic behavior: the volume change of the first coordination sphere of each metal center upon SCO is sensed by surrounding molecules through the crystal lattice.[3] Two strategies have been developed in order to promote communication between neighboring molecules: the polymeric approach is based on covalent linkages between metal centers, whereas the supramolecular approach uses weaker interactions such as H-bonding, $\pi-\pi$ stacking, or van der Vaals interactions. Although many supramolecular assemblies[4] and polymeric[5] compounds have already been investigated, the microscopic origin of cooperativity is not yet fully identified and in-depth studies of the structural and chemical factors controlling the characteristics of SCO are necessary to get a better understanding of the involved mechanism(s), and to design new systems that may be used in molecular electronics.[2]

In a related paper,[6] we have shown that $[FeL^A(NCS)_2]$ is LS and the materials in the series $[FeL^{Bx}(NCS)_2]$ are HS in the whole 5−400 K temperature range (L^A = tetradentate Schiff base resulting from 1:2 condensation between 2,2-dimethyl-1,3-diaminopropane and 2-acetylpyridine; L^{Bx} stands for the series of tetradentate Schiff bases *N*,*N*′-bis[(2-R-1*H*-imidazol-4-yl)methylene]-2,2-dimethylpropane-1,3-diamine, with R = H, Me, and Ph). By combining one pyridine and one imidazole ring in the same ligand, we have then prepared a new family of Fe^{II} complexes, $[FeL^{Cx}(NCS)_2]$, that include a dissymmetrical Schiff base ligand L^{Cx} (*N*-[(2-

* Corresponding author. E-mail: tuchague@lcc-toulouse.fr.
† Laboratoire de Chimie de Coordination du CNRS.
‡ On leave from the Institute of Applied Physics, Academy of Sciences of Moldova, Academiei Str. 3, 2028 Chisinau, Moldova.
§ Polish Academy of Sciences.

(1) (a) Goodwin, H. A. *Coord. Chem. Rev.* **1976**, *18*, 293. (b) Gütlich, P. *Struct. Bonding (Berlin)* **1981**, *44*, 83. (c) König, E.; Ritter, G.; Kulshreshtha, S. K. *Chem. Rev.* **1985**, *85*, 219. (d) Toftlund, H. *Coord. Chem. Rev.* **1989**, *94*, 67. (e) König, E. *Struct. Bonding (Berlin)* **1991**, *76*, 51. (f) Gütlich, P.; Hauser, A.; Spiering, H. *Angew. Chem.* **1994**, *106*, 2109; *Angew. Chem., Int. Ed.* **1994**, *33*, 2024. (g) Gütlich, P.; Goodwin, H. A. *Spin Crossover in Transition Metal Compounds I*; Topics in Current Chemistry; Springer-Verlag: Berlin, 2004; Vol. 233, p 1 and references therein. (h) Gaspar, A. B.; Ksenofontov, V.; Seredyuk, M.; Gütlich, P. *Coord. Chem. Rev.* **2005**, *249*, 2661.

(2) (a) Kahn, O.; Launay, J.-P. *Chemtronics* **1988**, *3*, 140. (b) Kahn, O.; Krober, J.; Jay, C. *Adv. Mater.* **1992**, *4*, 718. (c) Kahn, O.; Jay-Martinez, C. *Science* **1998**, *279*, 44. (d) Hayami, S.; Danjobara, K.; Inoue, K.; Ogawa, Y.; Matsumoto, N.; Maeda, Y. *Adv. Mater.* **2004**, *16*, 869. (e) Létard, J. F.; Guionneau, P.; Goux-Capes, L. In *Spin Crossover in Transition Metal Compounds*; Gütlich, P.; Goodwin, H. A., Eds.; Topics in Current Chemistry; Springer-Verlag: Berlin, 2004; Vol. 235; p 221.

(3) Spiering, H. *Spin Crossover in Transition Metal Compounds III*; Topics in Current Chemistry; Springer-Verlag: Berlin, 2004; Vol. 235, p 171 and references therein.

10.1021/cm061524m CCC: $33.50
Published on Web 10/21/2006

Chart 1. Schematic Drawing of $[FeL^{Dx}(NCX)_2]$

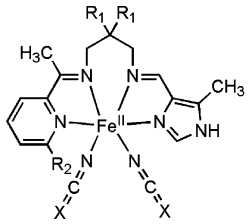

Complex	R_1	R_2	X
1: $[FeL^{D1}(NCS)_2].H_2O$	H	H	S
2: $[FeL^{D1}(NCSe)_2].H_2O$	H	H	Se
3: $[FeL^{D2}(NCS)_2]$	CH_3	H	S
4: $[FeL^{D2}(NCSe)_2]$	CH_3	H	Se
5: $[FeL^{D3}(NCS)_2]$	H	Br	S
6: $[FeL^{D4}(NCS)_2]$	CH_3	Br	S

R_2-1*H*-imidazol-4-yl)methylene]-*N*′1-pyridin-2-ylethylidene)-2,2-R_1-propane-1,3-diamine (R_1 = H and Me; R_2 = H, Me, and Ph). By minute modulations of the ligand, we have been able to monitor the spin state and observe different SCO behaviors, depending on the 2-R substituent of the imidazole ring.

Considering that the materials showing the most interesting SCO behavior were devoid of 2-R substituent, we decided to explore a series of materials including novel dissymmetrical ligands based on 5-methylimidazole-4-carboxaldehyde. In this new series, we also consider the effect of the coordinated NCSe vs NCS anions and the role of a bulky bromide substituent on the pyridyl moiety, with respect to the SCO properties of the resulting materials, which are summarized in the table associated with their schematic representation (Chart 1).

Experimental Section

Materials. All reagents (except 6-bromo-2-acetylpyridine) and solvents were commercially available (Aldrich) and were used without further purification.

Syntheses. ***Caution****: Although no such behavior was observed during the present work, perchlorate salts are potentially explosive and should be handled in small quantities and with much care.*

Chart 2. Schematic Drawing of 6-Bromo-2-acetylpyridine with NMR Labeling

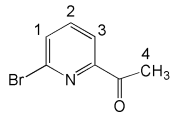

Chart 3. Schematic Drawing of the Half-Units L, L^{Br}, L′, and L'^{Br}

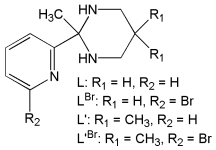

6-Bromo-2-acetylpyridine. This procedure was adapted from a literature method.[7] *N*,*N*′-dimethylacetamide (0.6 mL, 6 mmol) was added at 195 K to a solution of 6-bromo-2-lithiopyridine (obtained from 1.42 g of 2,6-dibromopyridine and 3.75 mL of a 1.6 N solution of *n*-butyllithium in ether (10 mL). The mixture was stirred for 2 h, during which the temperature slowly increased to 243 K, and the excess of *n*-butyllithium was then hydrolyzed with an aqueous solution of NH_4Cl (20 mL). The aqueous phase was separated and washed twice with ether (15 + 15 mL); the different fractions were gathered, dried on $MgSO_4$, and then evaporated to dryness. The obtained white powder was purified by column chromatography (silica (60−70−200 μm), with a 10:90 ethylacetate:pentane mixture as eluant), allowing us to isolate the 6-bromo-2-acetylpyridine as colorless crystals (yield: 1.1 g, 92%; see Chart 2).

Anal. Calcd for C_7H_6NOBr (200 g mol^{-1}): C, 42.03; H, 3.02; N, 7.00; Br, 39.95; O, 8.00. Found: C, 41.87; H, 2.76; N, 6.87; Br, 39.23; O, 7.81.

^{1}H NMR (250 MHz): δ 8.0 (dd, H1, J_3 = 6 Hz, J_5 = 0.8 Hz, 1H), 7.70 (dd, H2, J_3 = 6 Hz, J_3 = 6.5 Hz, 1H), 7.63 (dd, H3, J_3 = 6 Hz, J_5 = 0.8 Hz, 1H), 2.69 (s, H4, 3H).

Half-Units L, L^{Br}, L′, and L'^{Br}. The half-units (Chart 3) resulting from the Schiff base condensation of 2-acetyl-pyridine (6-bromo-2-acetylpyridine) and 1,3-diaminopropane for L (L^{Br}) or 2,2-dimethyl-1,3-diaminopropane for L′ (L'^{Br}) were synthesized as previously reported.[6]

Complexes. All complexation reactions and sample preparations for physical measurements were carried out in a purified nitrogen atmosphere inside a glovebox (Vacuum Atmospheres H.E.43.2) equipped with a dry train (Jahan EVAC 7).

General Procedure (1−6). To a pale yellow solution (1×10^{-3} mol, 10 mL methanol) of the aminal L (**1**, **2**), L′ (**3**, **4**), L^{Br} (**5**) or L'^{Br} (**6**) was slowly added a freshly prepared $Fe(NCS)_2$ solution[6,8] (1×10^{-3} mol, 10 mL methanol) with stirring. The reaction mixture immediately turned dark blue and was stirred for 5 more minutes. 5-Methylimidazole-4-carboxaldehyde (0.110 g, 1×10^{-3} mol, 10 mL methanol) was then added. No further color change was observed; the solution was stirred for 30 more minutes and then left undisturbed until a microcrystalline powder or crystals quantitatively formed.

*$[FeL^{D1}(NCS)_2]\cdot H_2O$ (**1**).* Dark blue powder. Yield: 0.32 g, 70%. Anal. Calcd for $FeC_{17}H_{21}N_7S_2O$ (459 g mol^{-1}): C, 44.45; H, 4.61; N, 21.34; S, 13.96; Fe, 12.15. Found: C, 44.84; H, 4.38; N, 21.05; S, 13.88; Fe, 12.15. IR (cm^{-1}): 2110−2090 (NCS); 1600 (imine). Mass spectrometry (FAB) calcd/found: 385.2906/383.0738 (FeL^{D2}-$(NCS)^+ + H_2O + NCS^-$). TGA: loss of ca. 2.8% (theor. 3.9%).

(4) (a) Lemercier, G.; Bousseksou, A.; Verelst, M.; Tuchagues, J.-P.; Varret, F. *J. Magn. Magn. Mater.* **1995**, *150*, 227. (b) Bousseksou, A.; Verelst, M.; Constant-Machado, H.; Lemercier, G.; Tuchagues, J.-P.; Varret, F. *Inorg. Chem.* **1996**, *35*, 110. (c) Lemercier, G.; Verelst, M.; Bousseksou, A.; Varret, F.; Tuchagues, J.-P. In *Magnetism : A Supramolecular Function*; Kahn, O., Ed.; NATO ASI Series C; Kluwer Academic Publishers: Dordrecht, The Netherlands, 1996; Vol. 484, p 335. (d) Thiel, A.; Bousseksou, A.; Verelst, M.; Varret, F.; Tuchagues, J.-P. *Chem. Phys. Lett.* **1999**, *302*, 549. (e) Hayami, S.; Gu, Z.; Shiro, M.; Einaga, Y.; Fujishima, A.; Sato, O. *J. Am. Chem. Soc.* **2000**, *122*, 7126. (f) Hayami, S.; Gu, Z.; Yoshiki, H.; Fujishima, A.; Sato, O. *J. Am. Chem. Soc.* **2001**, *123*, 11644. (g) Sunatsuki, Y.; Ikuta, Y.; Matsumoto, N.; Ohta, H.; Kojima, M.; Iijima, S.; Hayami, S.; Maeda, Y.; Kaizaki, S.; Dahan, F.; Tuchagues, J.-P. *Angew. Chem., Int. Ed.* **2003**, *42*, 1614. (h) Ikuta, Y.; Ooidemizu, M.; Yamahata, Y.; Yamada, M.; Osa, S.; Matsumoto, N.; Iijima, S.; Sunatsuki, Y.; Kojima, M.; Dahan, F.; Tuchagues, J.-P. *Inorg. Chem.* **2003**, *42*, 7001. (i) Yamada, M.; Ooidemizu, M.; Ikuta, Y.; Osa, S.; Matsumoto, N.; Iijima, S.; Kojima, M.; Dahan, F.; Tuchagues, J.-P. *Inorg. Chem.* **2003**, *42*, 8406. (j) Sunatsuki, Y.; Ohta, H.; Kojima, M.; Ikuta, Y.; Goto, Y.; Matsumoto, N.; Iijima, S.; Akashi, H.; Kaizaki, S.; Dahan, F.; Tuchagues, J.-P. *Inorg. Chem.* **2004**, *43*, 4154. (k) Salmon, L.; Bousseksou, A.; Donnadieu, B.; Tuchagues, J.-P. *Inorg. Chem.* **2005**, *44*, 1763. (l) Arata, S.; Torigoe, H.; Iihoshi, T.; Matsumoto, N.; Dahan, F.; Tuchagues J.-P. *Inorg. Chem.* **2005**, *44*, 9288.

(5) (a) Kröber, J.; Codjovi, E.; Kahn, O.; Grolière, F.; Jay, C. *J. Am. Chem. Soc.* **1993**, *115*, 9810. (b) Haasnoot, J. G. In *Magnetism : A Supramolecular Function*; Kahn, O., Ed.; NATO ASI Series C; Kluwer Academic Publishers: Dordrecht, The Netherlands, 1996; Vol. 484, p 299. (c) Real, J. A.; Gaspar, A. B.; Niel, V.; Muñoz, M. C. *Coord. Chem. Rev.* **2003**, *236*, 121. (d) Real, J.-A.; Gaspar, A. B.; Munoz, M.-C.; Gutlich, P.; Ksenofontov, V.; Spiering, H. *Spin Crossover in Transition Metal Compounds I*; Topics in Current Chemistry; Springer-Verlag: Berlin, 2004; Vol. 233, p 167 and references therein.

(6) Bréfuel, N.; Vang, I.; Shova, S.; Dahan, F.; Costes, J.-P.; Tuchagues, J.-P. *Polyhedron* **2006**, submitted.

(7) Parks, J. E.; Wagner, B. E.; Holm, R. H. *J. Organomet. Chem.* **1973**, *56*, 53.

(8) Erikson, N. E.; Sutin, N. *Inorg. Chem.* **1966**, *5*, 1834.

*[$FeL^{D1}(NCSe)_2$]·H_2O (**2**).* Dark blue powder. Yield: 0.33 g, 60%. Anal. Calcd for $FeC_{17}H_{21}N_7Se_2O$ (553 g mol^{-1}): C, 36.91; H, 3.83; N, 17.73; Se, 28.55; Fe, 10.10. Found: C, 37.23; H, 3.20; N, 17.61; Se, 28.02; Fe, 10.00. IR (cm^{-1}): 2110−2090 (NCS); 1600 (imine). TGA: loss of 3.4% (theor. 3.2%).

*[$FeL^{D2}(NCS)_2$] (**3**).* After 2 days, a dark blue precipitate was filtered off; 10 mL of acetonitrile were then added to the remaining solution. Slow crystallization (three weeks) yielded dark blue crystals suitable for X-ray analysis. Yield: 0.35 g, 75%. Anal. Calcd for $FeC_{19}H_{23}N_7S_2$ (469 g mol^{-1}): C, 48.62; H, 4.94; N, 20.89; S, 13.66; Fe, 11.90. Found: C, 48.51; H, 4.56; N, 20.36; S, 13.88; Fe, 11.50. IR (cm^{-1}; 297 K, LS state): 2111, 2072 (2 NCS absorptions); 1632(C═N imine); 1583 (C═N pyridine). IR (cm^{-1}; 343 K, HS state): 2110, 2072, 2031 (3 NCS absorptions). Mass spectrometry (FAB) calcd/found: 411.3285/411.1050 (FeL^{D2}-$(NCS)^+$ + NCS^-).

*[$FeL^{D2}(NCSe)_2$] (**4**).* Dark blue microcrystalline powder was obtained within a few days. Yield: 0.29 g, 52%. Anal. Calcd for $FeC_{19}H_{23}N_7Se_2$ (563 g mol^{-1}): C, 40.52; H, 4.12; N, 17.41; Se, 28.04; Fe, 9.92. Found: C, 40.37; H, 3.62; N, 16.98; Se, 27.29; Fe, 9.70. IR (cm^{-1}): 2110, 2090 (NCSe); 1600 (imine).

*[$FeL^{D3}(NCS)_2$] (**5**).* Black microcrystalline powder. Yield: 0.42 g, 80%. Anal. Calcd for $FeC_{17}H_{18}N_7S_2Br$ (520 g mol^{-1}): C, 39.25; H, 3.49; N, 18.85; S, 12.33; Fe, 10.74; Br, 15.36. Found: C, 39.18; H, 2.63; N, 18.50; S, 11.93; Fe, 10.56; Br, 15.12. IR (cm^{-1}): 2072, 2021 (NCS); 1646 (imine).

*[$FeL^{D4}(NCS)_2$] (**6**).* Black crystals suitable for X-ray analysis were obtained through slow crystallization (2 days). Yield: 0.410 g, 75%. Anal. Calcd for $FeC_{19}H_{22}N_7S_2Br$ (548 g mol^{-1}): C, 41.67; H, 4.04; N, 17.88; S, 11.69; Fe, 10.19; Br, 14.57. Found: C, 41.65; H, 3.54; N, 17.61; S, 11.10; Fe, 9.89; Br, 14.06. IR (cm^{-1}): 2070−2034 (NCS); 1641 (imine).

Physical Measurements. Elemental analyses were carried out on a Perkin-Elmer 2400 series II device (C, H, N) at the Microanalytical Laboratory of the Laboratoire de Chimie de Coordination in Toulouse, France, and on a Maxim Thermoelectron device (S, Fe) at the Service Central de Microanalyses du CNRS in Vernaison, France. One-dimensional ^1H and ^{13}C NMR spectra were performed on an AC 250 FT spectrometer (Bruker). Chemical shifts are given in parts per million versus TMS (^1H and ^{13}C) using $CDCl_3$ as solvent. IR spectra were measured in the 400−4000 cm^{-1} range on a 9800 FTIR spectrometer (Perkin-Elmer). Samples were run as KBr pellets. Mass spectra (FAB, fast atom bombarding) were recorded with a quadrupolar NERMAG R 10-10 instrument using an NBA matrix. Mössbauer spectra were recorded on a constant-acceleration conventional spectrometer with a 50 mCi source of ^{57}Co (Rh matrix), as previously described.[4k] A least-squares computer program[9] was used to fit the Mössbauer parameters and to determine their standard deviations of statistical origin (given in parentheses). Isomer shift values (δ) are relative to iron foil at 293 K. Variable temperature magnetic susceptibility data were collected on powdered samples on a MPMS-55 Quantum Design SQUID magnetometer or a Faraday type susceptometer under applied magnetic fields lower than 0.1 T. Diamagnetic corrections were applied by using Pascal's constants.

Crystallographic Data Collection and Structure Determination for 3 and 6. The crystallographic measurements for [FeL^{D2}-$(NCS)_2$] (**3**) were carried out with a Nonius Kappa CCD[10] diffractometer equipped with a graphite-monochromated Mo−K_α radiation source using ϖ rotations. Intensity data were collected from the same crystal, successively at 300, 350, 400, 200, and 100 K, using θ rotations with 2° frames and a detector-to-crystal distance of 35 mm. Monitoring of the collected data showed no significant intensity decrease in the whole temperature range. Preliminary orientation matrices and unit cell parameters were obtained from the peaks of the first 10 frames, respectively, and refined using the whole data set. Frames were integrated and corrected for Lorentz and polarization effects using DENZO.[11] The scaling as well as the global refinement of crystal parameters was performed with SCALEPACK.[11] Reflections partly measured on previous and following frames were used to scale these frames.

Diffraction data for [$FeL^{D4}(NCS)_2$] (**6**) were collected using an Oxford-Diffraction XCALIBUR CCD diffractometer equipped with a graphite-monochromated Mo-K_α radiation source. The crystal was placed 50 mm from the CCD detector. More than the hemisphere of reciprocal space was covered by a combination of four sets of exposures; each set had a different φ-angle (0, 90, 180, or 270° and each had an exposure of 40 s covering 0.75° in ω. Coverage of the unique set is 99.5% complete up to $2\theta = 52°$. The unit-cell determination and data integration were carried out using the CrysAlis package of Oxford Diffraction.[12]

All structures were solved by direct methods using SHELXS-86[13] or SHELXS-97[14] and refined by full-matrix least-squares on F_o^2 using SHELXL-97[15] with anisotropic displacement parameters for non-hydrogen atoms. For better fitting the electron density, we refined the positions of the carbon atoms in the diamino fragment of the ligand at 100, 200, and 300 K, taking into account disordered models, in combination with the available tools (PART, DFIX and SADI) of SHELXL-97.[15] The atoms belonging to the minor component of the disordered fragment were refined isotropically. The hydrogen atoms were placed geometrically and refined with the riding model ($U_{iso} = 1.2U_{atom\ of\ attachment}$). Scattering factors were taken from the standard compilation.[16] The molecular plots were obtained by using the ZORTEP program.[17] Absorption corrections were introduced by semiempirical methods on the basis of equivalent reflections, using the program MULTISCAN.[18] The final full-matrix least-squares refinement, minimizing $[\sum w(|F_o^2| - |F_c^2|)^2]$,[2] converged at the values of R and wR listed in Table 1, together with the main crystallographic parameters.

Results and Discussion

Syntheses. The 1:1 condensation reactions between 2-acetylpyridine or 6-bromo-2-acetylpyridine and 1,3-diaminopropane or 2,2-dimethyl-1,3-diaminopropane yielded the aminal type ligands L, 2-(2-methylhexahydro-2-pyrimidinyl)pyridine; L^{Br}, 2-(2-methylhexahydro-2-pyrimidinyl)-6-bromopyridine; L′, (2-(2-methyl-5-dimethylhexahydro-2-pyrimidinyl)-pyridine; and L'^{Br}, (2-(2-methyl-5-dimethylhexahydro-2-pyrimidinyl)-6-bromopyridine, respectively (first reaction

(9) Lagarec, K. *Recoil, Mössbauer Analysis Software for Windows*; http://www.physics.uottawa.ca/∼recoil.
(10) *Nonius (2201) COLLECT*; Nonius BV: Delft, The Netherlands.
(11) Otwinowski, Z.; Minor, W. Processing of X-ray Diffraction Data Collected in Oscillation Mode. In *Methods in Enzymology*; Carter, C. W., Sweet, R. M., Eds.; Academic Press: New York, 1997; Vol. 276: Macromolecular Crystallography, Part A, p 307.
(12) *CrysAlis RED*, version 1.170.32; Oxford Diffraction Ltd.: Oxford, U.K., 2003.
(13) Sheldrick, G. M. *SHELX86*; *Acta Crystallogr., Sect. A* **1990**, *46*, 467.
(14) Sheldrick, G. M. *SHELXS-97: Program for Crystal Structure Solution;* University of Göttingen: Göttingen, Germany, 1990.
(15) Sheldrick, G. M. *SHELXL-97: Program for the Refinement of Crystal Structures from Diffraction Data.* University of Göttingen: Göttingen, Germany, 1997.
(16) *International Tables for Crystallography*; Kluwer Academic Publishers: Dordrecht, The Netherlands, 1992; Vol. C.
(17) Zsolnai, L.; Pritzkow, H.; Huttner, G. *ZORTEP: Ortep for PC, Program for Molecular Graphics*; University of Heidelberg: Heidelberg, Germany, 1996.
(18) Blessing, R. H. *Acta Crystallogr., Sect. A* **1995**, *51*, 33.

Table 1. Crystallographic Data Collection and Structure Determination for Complexes 3 and 6

	$FeL^{D2}(NCS)_2$ (**3**)	$FeL^{D2}(NCS)_2$ (**3**)	$FeL^{D2}(NCS)_2$ (**3**)	$FeL^{D2}(NCS)_2$ (**3**)	$FeL^{D2}(NCS)_2$ (**3**)	$FeL^{D4}(NCS)_2$ (**6**)
formula	$C_{19}H_{23}FeN_7S_2$	$C_{19}H_{23}FeN_7S_2$	$C_{19}H_{23}FeN_7S_2$	$C_{19}H_{23}FeN_7S_2$	$C_{19}H_{23}FeN_7S_2$	$C_{19}H_{22}BrFeN_7S_2$
fw	469.41	469.41	469.41	469.41	469.41	548.32
cryst syst	triclinic	triclinic	triclinic	triclinic	triclinic	triclinic
space group	$P\bar{1}$	$P\bar{1}$	$P\bar{1}$	$P\bar{1}$	$P\bar{1}$	$P\bar{1}$
a (Å)	7.9120(11)	7.9371(11)	7.9860(12)	7.9487(5)	7.9769(8)	7.8186(16)
b (Å)	9.2150(15)	9.2656(15)	9.3410(16)	9.8685(9)	9.8759(12)	10.217(2)
c (Å)	14.860(2)	14.922(2)	14.9560(27)	14.6035(13)	14.6740(18)	14.314(3)
α (deg)	86.590(6)	86.736(6)	87.000(6)	91.109(3)	91.100(4)	91.00(3)
β (deg)	78.660(10)	78.692(10)	79.037(12)	98.639(5)	98.773(7)	95.67(3)
γ (deg)	86.460(11)	86.227(11)	85.846(11)	95.885(5)	95.976(7)	97.68(3)
V (Å^3)	1059.0(3)	1072.7(3)	1091.6(3)	1125.88(16)	1135.5(2)	1127.1(4)
Z	2	2	2	2	2	2
ρ_{calcd} (g cm^{-3})	1.472	1.453	1.428	1.385	1.373	1.616
λ (Å)	0.71073	0.71073	0.71073	0.71073	0.71073	0.71073
T (K)	100	200	300	350	400	180
μ(MoKα) (cm^{-1})	0.930	0.918	0.918	0.875	0.867	2.648
R^a [$I > 2\sigma(I)$]	0.0666	0.0595	0.0741	0.0700	0.0637	0.0437
wR^b	0.1326	0.1245	0.1559	0.1318	0.1277	0.0992

^{a} $R = \sum||F_o| - |F_c||/\sum|F_o|$. ^{b} $wR = [\sum w(|F_o^2| - |F_c^2|)^2/\sum w|F_o^2|^2]^{1/2}$.

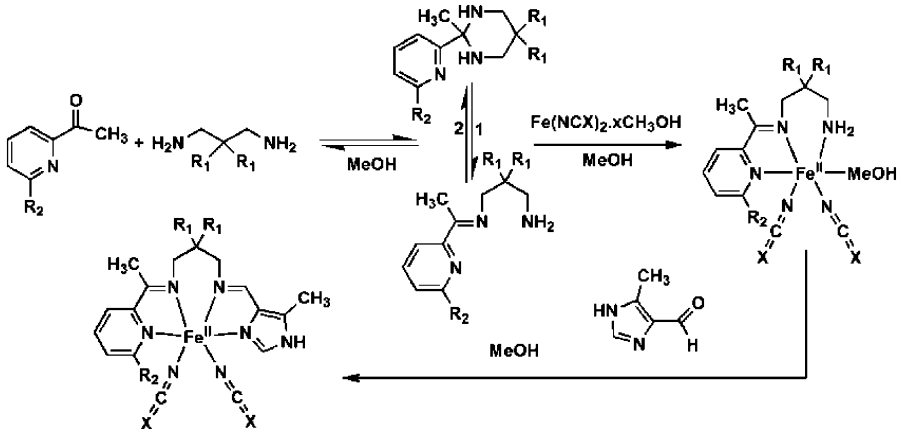

Figure 1. Synthetic pathway for the family of complexes $[FeL^{Dx}(NCX)_2]$ based on the dissymmetrical tetradentate Schiff base ligands L^{Dx} (R_1 = H, CH_3; R_2 = H, Br).

sketched in Figure 1). Clean and quantitative syntheses of the dissymmetrical ligands L^{Dx} could only be performed in the presence of $Fe(NCX)_2 \cdot x$MeOH yielding their $[FeL^{Dx}(NCX)_2]$ (X═S, Se; x = 1−4) complexes (Figure 1). As previously commented,[6] these results suggest that the metal ion totally displaces the equilibrium from the cyclic aminal toward the acyclic Schiff base intermediate through complexation according to the second reaction sketched in Figure 1.

Complexes 1 and 2. *Magnetic Properties.* The magnetic susceptibility of complex **1**, $[FeL^{D1}(NCS)_2] \cdot H_2O$, has been measured first in the warming mode between 300 and 400 K, in the cooling mode between 400 and 4 K, and finally in the warming mode between 5 and 400 K (Figure 2). At 300 K, the $\chi_M T$ product equals 0.43 cm^3 mol^{-1} K, indicating that Fe^{II} is in the LS state; upon the sample being warmed to 350 K, a slight increase in the $\chi_M T$ product is observed ($\chi_M T$ = 1 cm^3 mol^{-1} K at 350 K), and a relatively steep SCO then occurs within 25 K ($\chi_M T$ = 2.86 cm^3 mol^{-1} K at 376 K) corresponding to the dehydration of **1**, as further evidenced by thermogravimetric measurements, vide infra. Dehydration of the sample is almost complete after leaving the sample for 1 h at 400 K in the SQUID under reduced He pressure ($\chi_M T$ = 3.52 cm^3 mol^{-1} K). Upon subsequent cooling from 400 to 4 K, this sample, dehydrated in situ, shows a two-step SCO: the high-temperature step ($T^h_{1/2}\downarrow$ =

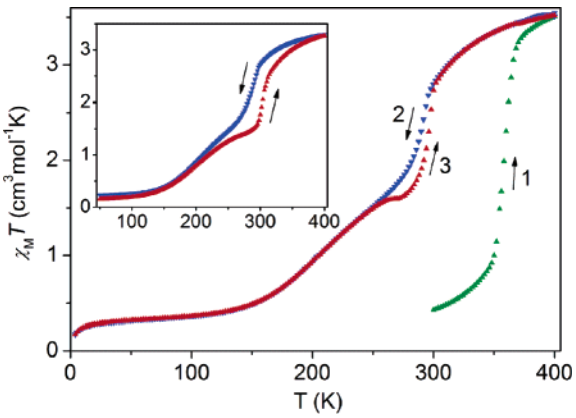

Figure 2. Thermal variation of the $\chi_M T$ product obtained for $[FeL^{D1}(NCS)_2] \cdot H_2O$, **1** (300−400 K branch), and $[FeL^{D1}(NCS)_2]$, the result from dehydration of **1** inside the SQUID at 400 K (consecutive 400−4 and 4−400 K branches). Insert: Thermal variation of the $\chi_M T$ product obtained for $[FeL^{D1}(NCS)_2]$, the result from dehydration of **1** under a vacuum.

292 K) is steep, whereas the subsequent low-temperature step ($T^l_{1/2} \approx$ 202 K) is gradual. Finally, upon this sample being warmed from 4 to 400 K, two steps, similar to those observed in the cooling mode, are successively observed with $T^l_{1/2} \approx$ 202 K and $T^h_{1/2}\uparrow$ = 298 K, evidencing a 6 K wide hysteresis loop for the high-temperature step.

To ascertain the unprecedented two-step SCO behavior of $[FeL^{D1}(NCS)_2]$, characterized by one smooth and one steep

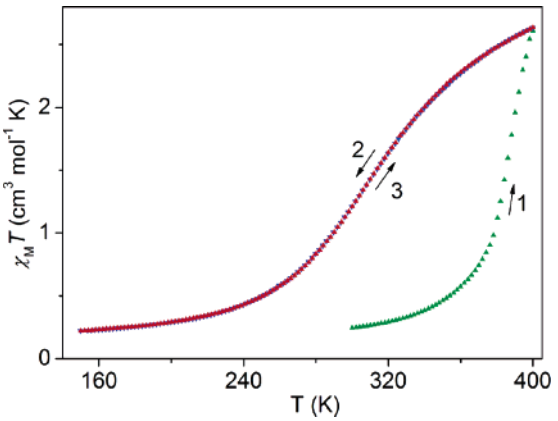

Figure 3. Thermal variation of the $\chi_M T$ product obtained for [FeL^{D1}(NCSe)$_2$]·H$_2$O, **2** (300−400 K branch), and for [FeL^{D1}(NCSe)$_2$], the result from dehydration of **2** inside the SQUID at 400 K (consecutive 400−150 and 150−400 K branches).

and hysteretic SCO,[19] we have also performed dehydration by warming a sample of **1** to 400 K under a vacuum for 12 h. The thermal $\chi_M T$ variation of this vacuum-dried sample, shown in the insert of Figure 2, shows a similar overall behavior, but with a wider hysteresis loop (11 vs 6 K) characterized by $T^h_{1/2}\downarrow = 292$ K and $T^h_{1/2}\uparrow = 303$ K.

Similarly, the magnetic susceptibility of complex **2**, [FeL^{D1}(NCSe)$_2$]·H$_2$O, has been measured first in the warming mode between 300 and 400 K, followed by the cooling mode between 400 and 150 K, and finally in the warming mode between 150 and 400 K (Figure 3). At 300 K, the $\chi_M T$ product is equal to 0.24 cm^3 mol^{-1} K, indicating that Fe^{II} is in the LS state; upon the sample being warmed to 374 K, a slight increase in the $\chi_M T$ product is observed ($\chi_M T = 0.84$ cm^3 mol^{-1} K at 374 K), and a relatively steep SCO then occurs within 26 K ($\chi_M T = 2.63$ cm^3 mol^{-1} K at 400 K) corresponding to the dehydration of **2**, as further evidenced by thermogravimetric measurements, vide infra. Although dehydration of the sample is complete at 400 K, the $\chi_M T$ product of 2.63 cm^3 mol^{-1} K indicates that the SCO is not yet complete at 400 K. Upon subsequent cooling from 400 to 150 K, this sample, dehydrated in situ, shows a one-step gradual SCO characterized by $T_{1/2} \approx 305$ K. Finally, upon this sample being warmed from 150 to 400 K, the same behavior as in the cooling mode is observed. The selenocyanate vs thiocyanate mass effect is dramatic, leading to a gradual one-step SCO for **2**, at variance with the two-step hysteretic SCO observed for **1**.

No color change is observed upon SCO of the dehydrated form of **1** and **2**. This may be ascribed to the presence of the pyridine aromatic ring conjugated with Fe^{II}, which results in a strong MLCT band that prevents observation of the expected thermochromism of **1** and **2**.[20]

Mössbauer Spectroscopy. Mössbauer spectra have been recorded at selected temperatures in the 80−400 K range for complex **1**. First, a sample of the hydrated material, [FeL^{D1}(NCS)$_2$]·H$_2$O, was cooled down to 80 K and its Mössbauer spectrum was recorded, yielding a single quadrupole split doublet characteristic of LS Fe^{II} (isomer shift, $\delta = 0.456(2)$ mm s^{-1}, and quadrupole splitting, $\Delta E_Q = 0.657(3)$ mm s^{-1}). The sample was then warmed to 400 K in the Mössbauer vacuum oven until complete dehydration was reached (monitored by conversion of the sample from the LS to the HS Fe^{II} state); Mössbauer spectra of [FeL^{D1}(NCS)$_2$] were then collected successively in the cooling and warming modes. Selected spectra are shown in Figure 4. The presence, in the dehydrated species, of two distinct iron(II) sites suggested by the two-step SCO evidenced by the magnetic study is confirmed by Mössbauer spectroscopy: comparison of the 80 K Mössbauer spectra 1 (initial hydrated sample) and 6 (after dehydration) clearly shows the presence of two LS Fe^{II} sites in the dehydrated sample (δ^A(LS) = 0.476(3) mm s^{-1} and $\Delta E_Q{}^A$(LS) = 0.69(2) mm s^{-1}, 46(4)%, and δ^B(LS) = 0.504(3) mm s^{-1} and $\Delta E_Q{}^B$(LS) = 1.08(2) mm s^{-1}, 46(4)%), at variance with the unique LS Fe^{II} site of the hydrated sample, vide supra. In the HS state, regardless of the temperature and of the high-spin fraction value, a_{HS}, sites A and B could not be distinguished; at 300 K, characteristic Mössbauer parameters include δ(HS) = 0.880(5) mm s^{-1} and ΔE_Q(HS) = 2.122(9) mm s^{-1}.

From the analysis of all other spectra (400−190 K in the cooling mode and subsequently 190−400 K in the warming mode), it is clear that the Fe^A site experiences SCO between 250 and 400 K, whereas the Fe^B site experiences SCO between 80 and 250 K. Furthermore, a comparative analysis of the spectra collected in the cooling and warming modes around 300 K clearly shows the occurrence of thermal hysteresis for the Fe^A site in this temperature range. It may then be concluded that loss of the crystallization water leads to a supramolecular reorganization distinguishing two different Fe^{II} sites in the dehydrated material.

It is worth mentioning that, regardless of the temperature, the HS doublet is unusually broad and that, in addition, it is asymmetric above 200 K, with either a more pronounced broadening of the v^+ absorption or a lower recoil-free fraction, *f*, than the v^- absorption. In the case of SCO materials, observation of Mössbauer spectra including broadened absorptions is usually related to dynamic phenomena: the interstate conversion rates K_{LH} (LS → HS) and K_{HL} (HS → LS) are comparable to the hyperfine frequency (10^8 s^{-1}).[4a,4d,21] In such a case, at temperatures where the LS to HS crossover is complete, the broadenings disappear and the HS spectra collected above this temperature are usually more or less symmetrical. Clearly, this is not the case of **1**, as the

(19) (a) Koppen, H.; Müller, E. W.; Köhler, C. P.; Spiering, H.; Meissner, P.; Gütlich, P. *Chem. Phys. Lett.* **1982**, *91*, 348. (b) Petrouleas, V.; Tuchagues, J.-P. *Chem. Phys. Lett.* **1987**, *137*, 21. (c) Boinnard, D.; Bousseksou, A.; Dworkin, A.; Savariault, J.-M.; Varret, F.; Tuchagues, J.-P. *Inorg. Chem.* **1994**, *33*, 271. (d) Garcia, Y.; Kahn, O.; Rabardel, L.; Chansou, B.; Salmon, L.; Tuchagues, J.-P. *Inorg. Chem.* **1999**, *38*, 4663. (e) Ksenofontov, V.; Gaspar, A. B.; Real, J. A.; Gütlich, P. *J. Phys. Chem. B* **2001**, 12266. (f) Nakano, K.; Kawata, S.; Yoneda, K.; Fuyuhiro, A.; Yagi, T.; Nasu, S.; Morimoto, S.; Kaizaki, S. *Chem. Commun.* **2004**, 2892. (g) Ksenofontov, V.; Gaspar, A. B.; Niel, V.; Reiman, S.; Real, J. A.; Gütlich, P. *Chem.—Eur. J.* **2004**, *10*, 1291. (h) Grunert, C. M.; Schweifer, J.; Weinberger, P.; Linert, W.; Mereiter, K.; Hilscher, G.; Müller, M.; Wiesinger, G.; van Koningsbruggen, P. J. *Inorg. Chem.* **2004**, *43*, 155. (i) Niel, V.; Thompson, A. L.; Goeta, A. E.; Enaschescu, C.; Hauser, A.; Galet, A.; Munoz, M. C.; Real, J. A. *Chem.—Eur. J.* **2005**, *11*, 2047.

(20) Létard, J.-F.; Guionneau, P.; Rabardel, L.; Howard, J. A. K.; Goeta, A. E.; Chasseau, D.; Kahn, O. *Inorg. Chem.* **1998**, *37*, 4432.

(21) (a) Hartmann-Boutron, F. *Ann. Phys.* **1975**, *9*, 285. (b) Adler, P.; Hauser, A.; Vef, A.; Spiering, H.; Gütlich, P. *Hyperfine Interact.* **1989**, *47*, 343. (c) Adler, P.; Spiering, H.; Gütlich P. *J. Chem. Phys.* **1989**, *50*, 587.

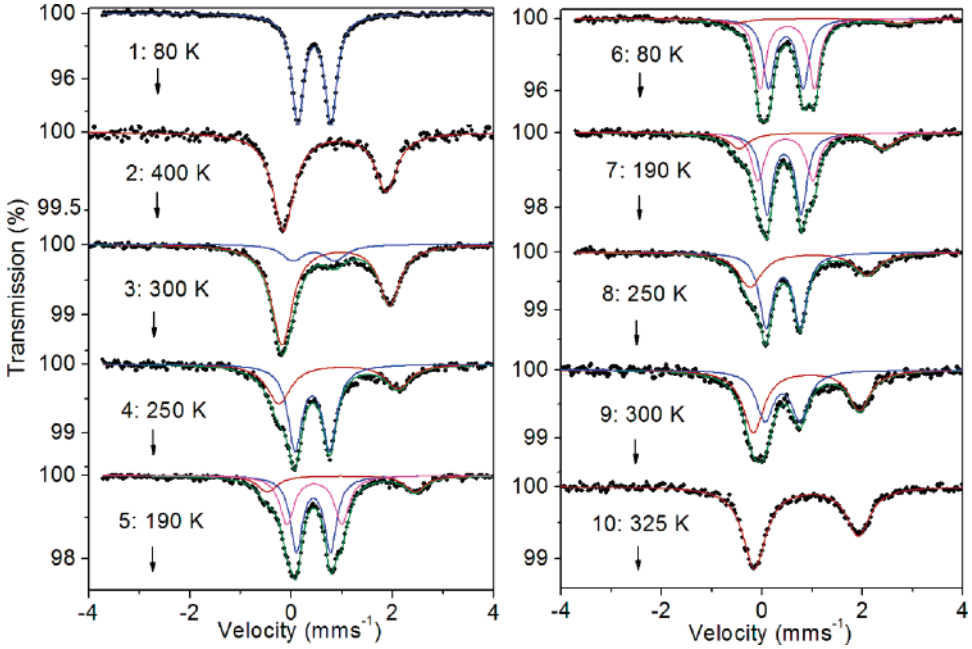

Figure 4. Selected Mössbauer spectra of **1**: spectrum 1, initial hydrated sample $[FeL^{D1}(NCS)_2]\cdot H_2O$; spectra 2−10, sample dehydrated in the Mössbauer vacuum oven, $[FeL^{D1}(NCS)_2]$; spectra 2−6, cooling mode, and spectra 7−10, warming mode.

line-broadenings of the purely HS phase increase with temperature. Texture effects[22] having been excluded by measuring a finely ground sample; this asymmetry may be associated with the anisotropy of thermally populated higher magnetic states.[23] However, in the absence of structural data, we cannot propose more detailed arguments. Another remarkable feature that emerged from the fitting of the Mössbauer spectra is that although two LS sites are clearly distinguished below 200 K, it is not possible to distinguish them even at moderately higher temperature (250 K), where the total LS fraction is still significantly large (>60%). This peculiarity may be associated with the line broadenings commented above.

Mössbauer spectra of complex **2** have been recorded at selected temperatures in the 80−400 K range. First, a Mössbauer spectrum of the hydrated material, $[FeL^{D1}(NCSe)_2]\cdot H_2O$, was recorded at 293 K, yielding a single quadrupole split doublet characteristic of LS Fe^{II} ($\delta = 0.366(6)$ mm s^{-1}, $\Delta E_Q = 0.624(9)$ mm s^{-1}). The sample was then warmed to 400 K in the Mössbauer vacuum oven until complete dehydration monitored by conversion of the sample from the LS state to constant a_{HS}%, and Mössbauer spectra of $[FeL^{D1}(NCSe)_2]$ were collected in the cooling mode. Selected spectra are shown in Figure 5. Analysis of the spectra indicates that although complete dehydration of the sample has been achieved (vide supra and the section below on thermogravimetry), conversion to the HS state is not yet complete at 400 K ($a_{HS} \approx 75\%$). Whereas the 80 K spectrum of the initially hydrated sample shows a single quadrupole split doublet and no residual HS fraction, after dehydration,

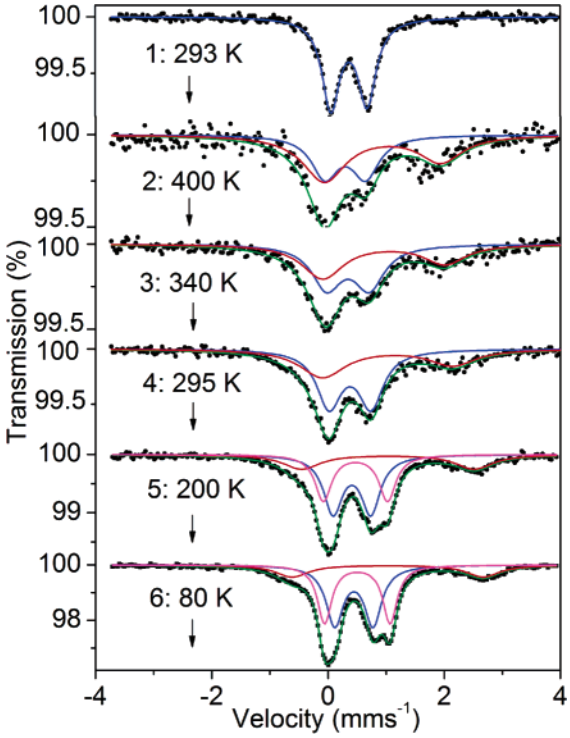

Figure 5. Selected Mössbauer spectra of **2**: spectrum 1, initial hydrated sample $[FeL^{D1}(NCSe)_2]\cdot H_2O$; spectra 2−6, sample dehydrated in the Mössbauer vacuum oven, $[FeL^{D1}(NCSe)_2]$, cooling mode.

the 80 K spectrum of this sample shows the presence of three quadrupole split doublets, two LS doublets (δ^A(LS) = 0.443(4) mm s^{-1} and $\Delta E_Q{}^A$(LS) = 0.66(2) mm s^{-1}, 45(3)%, and δ^B(LS) = 0.503(4) mm s^{-1} and $\Delta E_Q{}^B$(LS) = 1.127(9) mm s^{-1}, 37(3)%) and a residual HS fraction ($a_{HS} \approx 18\%$). Similar to **1**, in the HS state, regardless of the temperature and the a_{HS} value, sites A and B could not be distinguished; at 295 K, characteristic Mössbauer parameters include δ(HS) = 1.02(7) mm s^{-1} and ΔE_Q(HS) = 2.2(2) mm s^{-1}.

(22) (a) Henry, M.; Teillet, J.; Varret, F. *Rev. Phys. Appl.* **1980**, *15*, 1095. (b) Grandjean, F.; Long, G. J.; Benson, C. G.; Russo, U. *Inorg. Chem.* **1988**, *27*, 1524.
(23) (a) Londa, B.; Thalken, L.; Ceccarelli, C.; Glick, M.; Zhang, J. H.; Reiff, W. M. *Inorg. Chem.* **1983**, *22*, 1719. (b) Boudalis, A. K.; Clemente-Juan, J.-M.; Dahan, F.; Tuchagues, J.-P. *Inorg. Chem.* **2004**, *43*, 1574.

In spite of the poor counting statistics at high temperature (400−300 K), because of the strong absorption of the heavy selenium atom, this study confirms the smooth and incomplete SCO observed by magnetic measurements. Although it is clear from analysis of the spectra collected in the 295−80 K temperature range that the Fe^A site experiences SCO in a temperature range higher than that for the Fe^B site, at variance with **1** and in agreement with the magnetic susceptibility measurements, it is not possible to distinguish two steps in the SCO of **2**. However, similar to the case of **1**, it may be concluded that loss of the crystallization water leads to a supramolecular reorganization, distinguishing two different Fe^{II} sites in the dehydrated material.

As in the case of **1**, regardless of the temperature, the HS doublet is unusually broad and, in addition, it is asymmetric above 200 K, with either a more pronounced broadening of the v^+ absorption or a lower recoil-free fraction, *f*, than the v^- absorption. At variance with the case of **1**, there is still a significant LS fraction at 400 K; it is thus not possible to exclude that the interstate conversion rates may be comparable to the hyperfine frequency. This asymmetry may thus be associated with either dynamic phenomena or the anisotropy of thermally populated higher magnetic states.[23] As for **1**, although two LS sites are clearly distinguished up to 200 K, it is not possible to distinguish them at higher temperature.

Thermogravimetry. Thermogravimetric analyses have been performed on **1** and **2**, in order to monitor the loss of water at high temperature. The relative loss of mass measured upon heating **1** is ca. 2.8%, which, although lower, is close to the theoretical value of 3.9% calculated for the loss of one water molecule per mole of complex. Under a flow of dried air, rehydration is very slow, but it becomes faster under a flow of undried air. The dehydrated form, $[FeL^{D1}(NCS)_2]$, is not stable in the presence of moisture; rehydration occurs rapidly in a first step, and then becomes slower as rehydration increases. The 20 °C isotherm shows that this process is nearly complete after 15 h.

A similar study has been carried out for **2**. The relative loss of mass measured upon heating **2** is ca. 3.4%, close to the theoretical value of 3.2% calculated for the loss of one water molecule. The rehydration is slow under a flow of dried air, but becomes much faster under a flow of undried air; similar to complex **1**, the dehydrated form of **2** is not stable in the presence of moisture, but rehydration is more progressive, although the 20 °C isotherm shows that the process is nearly complete after 15 h.

Complexes 3 and 4. *Magnetic Properties.* The magnetic susceptibility of complex **3**, $[FeL^{D2}(NCS)_2]$, has been measured first in the warming mode between 150 and 400 K, and then in the cooling mode between 400 and 150 K (Figure 6). At 150 K, the value of the $\chi_M T$ product is equal to 0.15 $cm^3\ mol^{-1}K$, indicating that Fe^{II} is in the LS state, as confirmed by Mössbauer spectroscopy (vide infra); upon the sample being warmed, a slight increase in the $\chi_M T$ product is observed between 270 and 315 K ($\chi_M T = 0.79\ cm^3 mol^{-1}$ K at 315 K), and then, from 315 K, a steep SCO occurs within 2 K ($\chi_M T = 2.17\ cm^3\ mol^{-1}$ K at 317 K). This LS to HS crossover is incomplete and the $\chi_M T$ product slightly

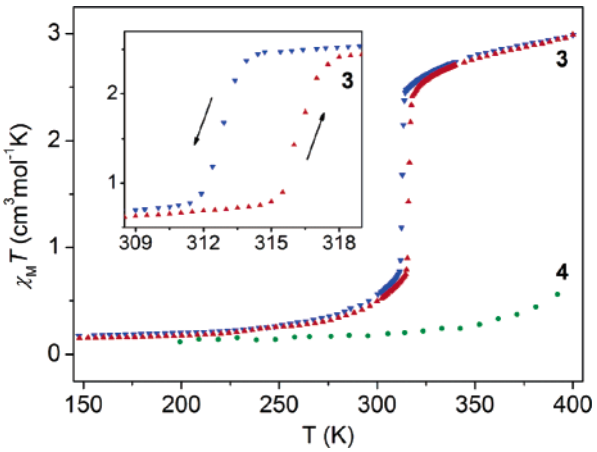

Figure 6. Thermal variation of the $\chi_M T$ product for complexes **3** and **4**. Insert: Magnification of the hysteresis loop of complex **3**.

increases, up to 2.99 $cm^3\ mol^{-1}K$ at 400 K. Upon subsequent cooling from 400 to 150 K, HS to LS crossover occurs at 313 K, evidencing a 4 K wide hysteresis loop, which suggests efficient cooperative interactions between adjacent molecules in this material. As previously mentioned for **1** and **2**, no color change is observed upon SCO of **3**, which also includes a pyridine aromatic ring conjugated with Fe^{II}.[20] Upon light irradiation of **3** at 5 K with different laser wavelengths, the LIESST effect[24] was not observed. In agreement with the inverse-energy-gap law, this may be related to the high $T_{1/2}$ value.[25] However, several compounds with $T_{1/2}$ values close to 300 K have recently been shown to exhibit LIESST,[26] and the "coordination degree of the ligand involved in the inner coordination sphere" has been suggested to play a prominent role toward T_0.[27] The tetradentate L^{D2} ligand should then endow **3** with a T_0 value intermediate between those for the $[Fe(bpp)_2]X_2 \cdot nH_2O$ series[26b] and $[Fe(L)(CN)_2] \cdot H_2O$[26a] (bpp is the tridentate ligand 2,6-bis(pyrazol-3-yl)-pyridine and L is the pentadentate macrocyclic Schiff base derived from condensation of 2,6-diacetylpyridine with 3,6-dioxaoctane-1,8-diamine). According to this rationale and considering the T_0 limiting values of 150 and 180 K,[27] applying $T_{LIESST} = T_0 - 0.3T_{1/2}$ with $T_{1/2} = 315$ K yields the limiting "theoretical" T_{LIESST} values of 56 and 86 K for **3**. It is thus clear that factors other than the coordination degree of the ligand also play a significant role toward T_0.

At variance, complex **4**, $[FeL^{D2}(NCSe)_2]$, remains LS in the whole temperature range, with a very slight increase in the $\chi_M T$ product above 350 K that can be attributed to the onset of SCO (Figure 6).

Mössbauer Spectroscopy. Mössbauer spectra have been recorded at selected temperatures in the 80−330 K range for complex **3**. First, the sample of $[FeL^{D2}(NCS)_2]$ was cooled

(24) (a) Descurtins, S.; Gütlich, P.; Köhler, C. P.; Spiering, H.; Hauser, A. *Chem. Phys. Lett.* **1984**, *13*, 1. (b) Descurtins, S.; Gütlich, P.; Hasselbach, K. M.; Spiering, H.; Hauser, A. *Inorg. Chem.* **1985**, *24*, 2174.
(25) (a) Hauser, A. *Coord. Chem. Rev.* **1991**, *111*, 275. (b) Hauser, A. *Spin Crossover in Transition Metal Compounds II*; Topics in Current Chemistry; Springer-Verlag: Berlin, 2004; Vol. 234, p 155.
(26) (a) Hayami, S.; Gu, Z.-Z.; Einaga, Y.; Kobayasi, Y.; Ishikawa, Y.; Yamada, Y.; Fujishima, A.; Sato, O. *Inorg. Chem.* **2001**, *40*, 3240. (b) Marcén, S.; Lecren, L.; Capes, L.; Goodwin, H. A.; Létard, J.-F. *Chem. Phys. Lett.* **2002**, *358*, 87.
(27) Létard, J.-F. *J. Mater. Chem.* **2006**, *16*, 2550.

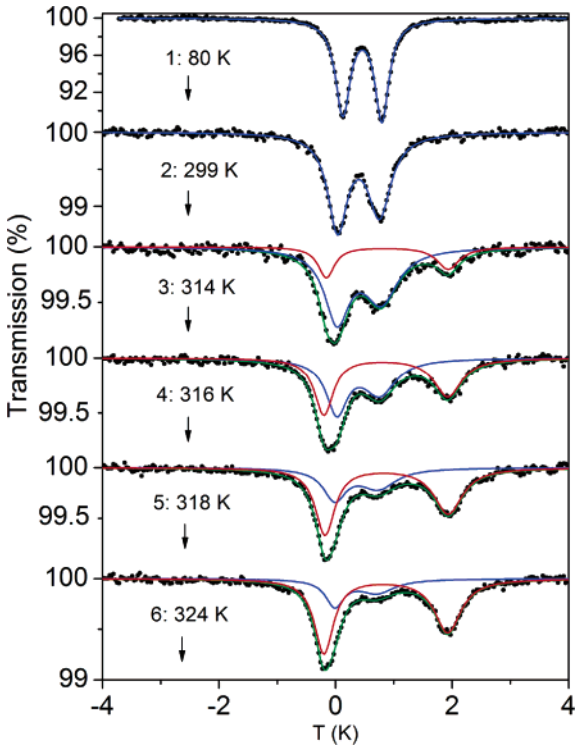

Figure 7. Selected Mössbauer spectra of complex **3**, $[FeL^{D2}(NCS)_2]$.

down to 80 K and its Mössbauer spectrum was recorded, yielding a single quadrupole split doublet characteristic of LS Fe^{II} ($\delta = 0.460(2)$ mm s^{-1} and $\Delta E_Q = 0.671(3)$ mm s^{-1}). The sample was then warmed to 295 K and transferred to the Mössbauer vacuum oven, where Mössbauer spectra were collected in the warming mode at several temperatures spanning the 295−324 K range. Selected spectra are shown in Figure 7. Comparative analysis of the spectra collected in this temperature range clearly shows the occurrence of a very steep SCO around 316 K (Figure 7), as previously observed through magnetic susceptibility measurements.

At variance with the case of **1** and **2**, and except for the 80 K spectrum, both the LS and HS doublets are broad and asymmetric over the whole 295−324 K range. In the 295−312 K range, the spectra are characterized by the presence of a unique LS doublet, and its broadening and dissymmetry may be ascribed to the onset of dynamic phenomena. This interpretation is supported by the slight increase in the $\chi_M T$ product observed between 270 and 313 K (previous subsection). At variance with the case of **1** and similarly to the case of **2**, there is still a significant LS fraction at 400 K, but both the dominant HS fraction and the residual LS one are broadened above 312 K. It is thus likely that the asymmetry and line broadenings may be associated with dynamic phenomena originating from interstate conversion rates comparable to the hyperfine frequency in complex **3**.[22]

Thermodynamical Parameters. Differential scanning calorimetry (DSC) measurements have been carried out for complex **3**, $[FeL^{D2}(NCS)_2]$, between 180 and 415 K at heating and cooling rates of 10 K min^{-1}. The transition temperatures $T\uparrow = 316$ K and $T\downarrow = 308$ K indicate occurrence of an 8 K wide hysteresis (Figure 8). Considering the difference in sweeping rates among the two techniques, these values match nicely with those deduced from the $\chi_M T$ data.

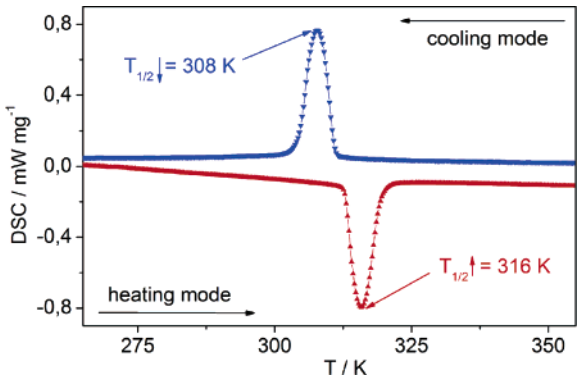

Figure 8. Differential scanning calorimetry (DSC) for complex **3**, $[FeL^{D2}(NCS)_2]$, in the heating and cooling modes.

The overall enthalpy (ΔH) and entropy (ΔS) variations associated with this hysteretic SCO determined from the DSC curves are $\Delta H\uparrow = -8.4 \pm 0.1$ kJ mol^{-1}, $\Delta S\uparrow = -27 \pm 1$ J K^{-1} mol^{-1}, and in the cooling mode $\Delta H\downarrow = 8.7 \pm 1$ kJ mol^{-1}, $\Delta S\downarrow = 28 \pm 1$ J K^{-1} mol^{-1}. The ΔS values are slightly smaller than those reported in the literature for mononuclear systems (∼30−80 J $K^{-1}mol^{-1}$), although they are larger than the ΔS variation associated with the spin-state change $\Delta S_{el} = R\ln[(2S+1)_{HS}/(2S+1)_{LS}] = 13.4$ J K^{-1} mol^{-1} for iron(II) complexes. The excess of entropy (around 15 J K^{-1} mol^{-1}) corresponds to the changes in intramolecular (essentially the $[FeN_6]$ core) and intermolecular vibrations (network vibrations: phonon entropy)[28] as well as the dynamics of the propylene fragment upon LS ↔ HS crossover (vide infra).[29]

Consistency between the magnetic and thermodynamic data has been checked using the regular solution model expressed as follows

$$\ln[(1-\gamma_{HS})/(\gamma_{HS}-f_{HS})] = [\Delta H + \Gamma(f_{HS}+1-2\gamma_{HS})]/RT - \Delta S/R$$

where ΔH and ΔS are the average values obtained from DSC measurements (cooling and warming modes) and Γ is the parameter accounting for the cooperativity associated with SCO. γ_{HS} and f_{HS} are defined as $\gamma_{HS} = (\chi_M T)_T/(\chi_M T)_{HS}$ and $f_{HS} = (\chi_M T)_{LT}/(\chi_M T)_{HS}$, respectively.[30] $(\chi_M T)_T$ is the value of $\chi_M T$ at any temperature, $(\chi_M T)_{HS}$ corresponds to the pure HS state and $(\chi_M T)_{LT}$ corresponds to the value of $\chi_M T$ at low temperature, once SCO has occurred. In the present case, $(\chi_M T)_{LT}$ is 0.15 cm^3 K mol^{-1} ($f_{HS} \approx 0.05$).

Figure 9 displays the steady-state curve (dotted line) computed using the above-mentioned model. A satisfactory fit has been obtained by setting ΔH, ΔS, and f_{HS} close to the experimental values (8.2 kJ mol^{-1}, 26 J $K^{-1}mol^{-1}$, and 0.020, respectively). Least-squares fitting leads to the interaction parameter $\Gamma = 5.7$ kJ mol^{-1}, which is, as expected, larger than $2RT_c$ ($T_c = 315$ K) and accordingly fulfills the condition for observing hysteresis.[30]

(28) Tuchagues, J.-P.; Bousseksou, A.; Molnár, G.; McGarvey, J. J.; Varret F. In *Spin Crossover in Transition Metal Compounds III*; Gütlich, P., Goodwin, H. A., Eds.; Topics in Current Chemistry; Springer-Verlag: Berlin, 2004; Vol. 235, p 85 and references therein.
(29) Sorai, M.; Nakano, M.; Miyazaki, Y. *Chem. Rev.* **2006**, *106*, 976.
(30) Galet, A.; Munoz, M. C.; Gaspar, A. B.; Real, J. A. *Inorg. Chem.* **2005**, *44*, 8749.

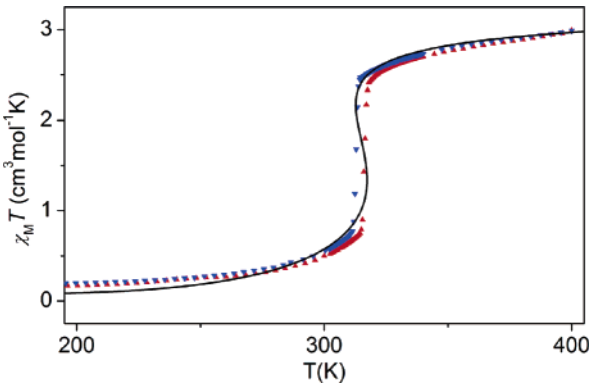

Figure 9. Numerical simulations of the magnetic behavior of complex **3**, $[FeL^{D2}(NCS)_2]$ (black line = steady states curve).

Variable-Temperature IR Studies. Variable-temperature IR spectroscopy is a valuable technique for monitoring SCO: in general, a significant increase in the Fe−L stretching vibrations is observed in the near IR upon HS → LS crossover, from ∼250 cm^{-1} for the HS state to ∼400 cm^{-1} for the LS state.[31] Moreover, the N−C(S/Se) stretching modes around 2000 cm^{-1} are very sensitive to the spin-state of Fe^{II} SCO complexes, including N-coordinated pseudohalides such as NCS or NCSe: upon HS−LS crossover, the corresponding absorption is shifted ca. 40 cm^{-1} toward higher frequencies.[31] Complex **3** has been studied using this technique at 293 K (LS state) and 350K (HS state), focusing on the 2000−2200 cm^{-1} spectral area. The LS state is characterized by two absorptions (2125 and 2113 cm^{-1}). In agreement with magnetic susceptibility that shows the presence of a small HS fraction at ambient temperature, we attribute the band at 2072 cm^{-1} (and the weak and partially hidden absorption around 2030 cm^{-1}) to the HS species. At 350 K, where the material is essentially HS, the intensity of the HS absorptions (2071 and 2031 cm^{-1}) is larger than that of the absorptions (2124 and 2111 cm^{-1}) arising from the LS residual fraction. These IR data confirm the thermally induced SCO observed by magnetic measurements, Mössbauer spectroscopy, and calorimetric studies.

Crystal Structure of Complex 3. Because of the thermal stability of $[FeL^{D2}(NCS)_2]$, **3**, over a large temperature range, it was possible to collect X-ray data in both the LS (100, 200, and 300 K) and HS (350 and 400 K) states. **3** crystallizes in the same $P\bar{1}$ space group in whole 100−400 K temperature range, regardless of the LS or HS state of Fe^{II} (Table 1). However, remarkable differences in the Fe−N bond lengths and bond angles (Table 2), as well as in the arrangement of the complex molecules in the crystal, have been observed between the LS and HS phases.

The molecular structure of the neutral complex **3**, $[FeL^{D2}(NCS)_2]$, at 100 and 400 K is depicted in Figure 10. The distorted Fe^{II} octahedral coordination sphere includes four equatorial nitrogen atoms of the tetradentate ligand L^{D2} and two apically coordinated NCS^- anions. The average Fe−N bond length increases from 1.965(8) Å at 300 K to 2.163(5) Å at 350 K, clearly indicating that **3** is essentially in the LS state at 300 K and below, whereas it is essentially in the HS state at 350 K and above.

Table 2. Selected Bond Lengths (Å) and Bond Angles (deg) for Complex 3, $[FeL^{D2}(NCS)_2]$, at 300 K (predominant LS State) and 350 K (predominant HS State)

	length (Å)			angle (deg)	
Fe−N	300 K	350 K	N−Fe−N	300 K	350 K
Fe−N1	2.061(4)	2.173(4)	N1−Fe−N5	89.50(17)	89.84(15)
Fe−N2	1.975(4	2.112(4)	N2−Fe−N3	94.98(17)	90.81(14)
Fe−N3	1.959(4)	2.143(3)	N2−Fe−N4	174.89(18)	164.83(14)
Fe−N4	1.977(4)	2.124(4)	N2−Fe−N5	89.68(18)	100.89(17
Fe−N5	1.953(5)	2.068(4)	N2−Fe−N6	94.93(19)	85.02(16)
Fe−N6	1.946(5)	2.344(5)	N5−Fe−N6	175.22(18)	173.39(18)

In the 300−350 K temperature range, **3** undergoes a LS → HS crossover, accompanied by a significant change of the lattice parameters (Table 1) due to thermal dilatation and lengthening of the Fe−N distances. As expected, the unit-cell volume increases from 1059.0(3) $Å^3$ at 100 K to 1135.5-(2) $Å^3$ at 400 K, which constitutes a 7.2% increase (76.5 $Å^3$). The most significant change, 0.398 Å, is observed for the Fe−N6 bond length, which increases from 1.946(5) Å at 300 K to 2.344(5) Å at 350 K, whereas changes for the remaining Fe−N bonds fall within the 0.11−0.18 Å range. Also, in the same temperature range, changes in N−Fe−N bond angles are not homogeneous: three N−Fe−N angles corresponding to one six-membered and two five-membered metallacycles decrease by values ranging from 2.29 to 4.45°, whereas the N1−Fe−N4 angle increases by 9.98°. Accordingly, whereas the iron atom deviates from the mean equatorial plane only by 0.059 Å at 100 K, this deviation increases up to 0.161 Å at 400 K.

The sum $\sum$ of the deviations from 90° of the 12 cis angles in the coordination sphere[32] may be used to characterize the average angular distortion of the coordination octahedron upon SCO through the n_Σ ratio of the $\sum_{HS}$ to $\sum_{LS}$ values,[33] or through the difference $\Delta = \sum_{HS} - \sum_{LS}$.[34] In the case of **3**, $\sum_{HS} = 84.4°$ and $\sum_{LS} = 53°$, leading to $n_\Sigma = 1.59$ and $\Delta\sum = 31.4°$. These values are within the ranges reported for these parameters for $[Fe(L_n)(NCS)_2]$ complexes[33,34] (L = mono- ($n = 4$), bi- ($n = 2$), and tetradentate ($n = 1$) nitrogen ligands) although the NCS^- anions of **3** are trans-coordinated and L^{D2} is linear tetradentate, whereas in the $[Fe(L_n)(NCS)_2]$ series reported,[33,34] the NCS^- anions are cis-coordinated and the two tetradentate ligands involved are tripodal.

The tetradentate ligand of **3** is in a similar configuration at all temperatures. The dihedral angle defined by the pyridine and imidazole moieties is comprised between 4.9

(31) (a) Nakamoto, K. *Infrared and Raman Spectra of Inorganic and Coordination Compounds*, 4th ed.; John Wiley & Sons: New-York, 1986. (b) Müller, E. W.; Ensling, J.; Spiering, H.; Gütlich, P. *Inorg. Chem.* **1983**, *22*, 2074. (c) Herber, R. H. *Inorg. Chem.* **1987**, *26*, 173. (d) Figg, D. C.; Herber, R. H. *Inorg. Chem.* **1990**, *29*, 2170. (e) Bousseksou, A.; McGarvey, J. J.; Varret, F.; Real, J. A.; Tuchagues, J. P.; Dennis, A. C.; Boillot, M. L. *Chem. Phys. Lett.* **2000**, *318*, 409.

(32) (a) Drew, M. G. B.; Harding, C. J.; McKee, V.; Morgan, G. G.; Nelson, J. *J. Chem. Soc., Chem. Commun.* **1995**, 1035. (b) Deeney, F. A.; Harding, C. J.; Morgan, G. G.; McKee, V.; Nelson, J.; Teat, S. J.; Clegg, W. *J. Chem. Soc., Dalton Trans.* **1998**, 1837.

(33) Guionneau, P.; Brigoulex, C.; Barrans, Y.; Goeta, A. E.; Létard, J.-F.; Howard, J. A. K.; Gaultier, J.; Chasseau, D. *C. R. Acad. Sci. Paris* **2001**, *C4*, 161.

(34) Guionneau, P.; Marchivie, M.; Bravic, G.; Létard, J.-F.; Chasseau, D. In *Spin Crossover in Transition Metal Compounds*; Gütlich, P., Goodwin, H. A., Eds.; Topics in Current Chemistry; Springer-Verlag: Berlin, 2004; Vol. 234, p 97.

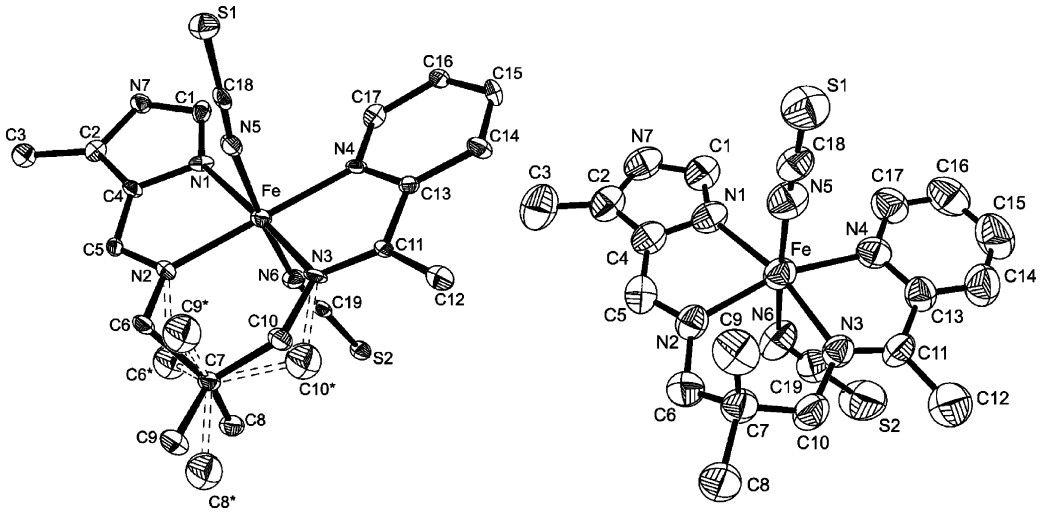

Figure 10. Left: ORTEP view of complex **3**, $[FeL^{D2}(NCS)_2]$, at 100 K. The minor component of the disordered fragment is drawn with broken lines. Right: ORTEP view of complex **3** at 400 K. Thermal ellipsoids are drawn at the 40% probability level.

(100 K) and 16.5° (400 K). Two five-membered metallacycles, FeN1C4C5N2 and FeN4C13C11N3, have a planar configuration with atom departures from their least-square plane smaller than the estimated standard deviation. The FeN2C6C7C10N3 six-membered metallacycle has a configuration that may rather be described as half-boat, with C7 departing by 0.67−0.69 Å from the almost planar FeN2C10C6N3 fragment in the whole 100−400 K temperature range.

However, at 100, 200, and 300 K (LS state), the C6 and C10 carbon atoms involved in this metallacycle (and consequently C8 and C9) are disordered over two well-resolved positions (Figure 10, left). Population of the major component in the structure decreases with increasing temperature from 90% at 100 K to 83% at 300 K. The minor component is characterized by a well-defined chair conformation of the FeN2C6C7C10N3 metallacycle. However, at higher temperatures (350 and 400 K), the difference electron density maps around the C6, C7, C8, C9, and C10 atoms clearly indicate only one position for each atom, which corresponds exactly to the position of the major component at low temperatures (Figure 10, right). It may be concluded that the thermal LS to HS crossover is concomitant to the disappearance of a statistical disorder in the propyl fragment of L^{D2}.

As noted above, the crystal packing of **3** in the HS and LS states is quite different. The crystal packing for the low-temperature phase is shown in Figure 11. Two types of significant short intermolecular contacts determine the structural motif at 100, 200, and 300 K: (i) the H-bond between N7 (imidazole) and S1 (NCS) of an adjacent complex molecule (N7···S1′ ($x - 1, y, z$) = 3.370(4) (3.406(5)) Å and N7−H···S1′ = 126.1 (126.8)°, for 100 and 300 K, respectively). These H-bonds link the complex molecules into infinite chains propagating along *a*; (ii) the $\pi-\pi$ stacking interaction between neighboring H-bonded chains. This is evidenced by the short interplanar distance (3.45 Å) between overlapping centrosymmetrically related imidazole rings, leading to ribbons, as illustrated in Figure 11. Additional intermolecular C−H···S contacts involving atom S2 with

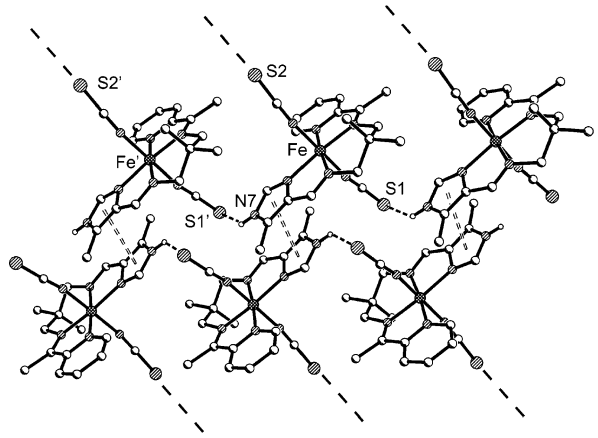

Figure 11. Fragment of an infinite ribbon in the crystal structure of **3** at 100, 200, and 300 K. Broken lines departing from S2 atoms suggest the 2D layered structure of **3**.

C···S separations ranging from 3.66 to 3.95 Å appear to be significantly weak.[35] However, the S2···S2′ ($-x, 1 - y, 1 - z$) short contact, 3.493(3) Å at 100 K and 3.578(3) Å at 300 K,[36] determines extension of the above-mentioned ribbons into a 2D supramolecular architecture (Figure 11).

In the high-temperature phase at 350 and 400 K, no N−H···S bonds have been found. Instead, the strongest interaction between adjacent complex molecules in the crystal involves a short intermolecular contact between N7(imidazole) and N6(NCS^-) (N7···N6′ ($2 - x, 1 - y, 1 - z$) = 3.008(6) (3.024(5)) Å and N7−H···N6′ = 149.8 (149.4°) at 350 and 400 K, respectively). Obviously, this is the reason for the lengthening of the Fe1−N6 bond length and for the decrease in the N6−Fe−C19 bond angle from 170.6(4)° at 300 K to 134.3(4)° at 350 K (Table 2). The change in H-bond network upon crossover from the LS to HS phase results in the association of the neutral $[FeL^{D2}(NCS)_2]$ complex molecules into centrosymmetric dinuclear species, as shown

(35) (a) Desiraju, G. R.; Nalini, V. *J. Mater. Chem.* **1991**, *1*, 201. (b) van Derberg, J.-A.; Seddon K. R. *Cryst. Growth Des.* **2003**, *3*, 643. (c) Desiraju G. R. *Chem. Commun.* **2005**, 2995.
(36) Takahashi, K.; Kawakami, T.; Gu, Z.; Einaga, Y.; Fujishima, A.; Sato, O. *Chem. Commun.* **2003**, 2375.

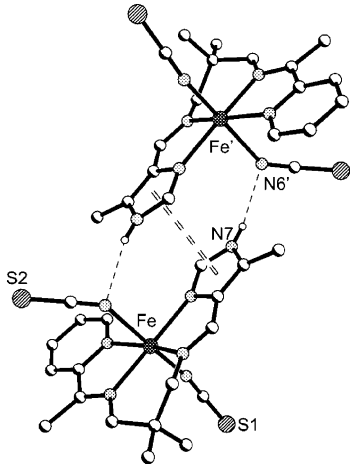

Figure 12. Centrosymmetric H-bonded dinuclear species in the crystal structure of **3**, [FeL^{D2}(NCS)$_2$], at 350 and 400 K. Nonrelevant hydrogen atoms are omitted for clarity.

in Figure 12. Consequently, the $\pi-\pi$ interaction between imidazole moieties is realized inside each pair of complex molecules resulting in a supramolecular structure considerably less extended in the HS than in the LS phase.

The main crystal packing motif in the HS phase (350 and 400 K) is an arrangement of zigzag infinite chains parallel to the [011] direction. Each chain is built from dinuclear {[FeL^{D2}(NCS)$_2$]}$_2$ H-bonded species (Figure 12) associated through the short S2···S2 ($2 - x, -y, -z$) contact[36] (3.625(3) Å at 350 K and 3.653(3) Å at 400 K), which is quite similar to that observed in the low-temperature phase at 100, 200, and 300 K.

Complexes 5 and 6. *Magnetic Properties.* Complexes **5**, [FeL^{D3}(NCS)$_2$], and **6**, [FeL^{D4}(NCS)$_2$], are HS species, as indicated by their constant $\chi_M T$ product over the whole 80−300 K temperature range explored (3.9 and 4.1 cm^3 mol^{-1} K at 80 K, respectively). This clearly shows that combination of the steric and electronic effects of the 6-bromo substituent introduced on the pyridyl ring of the ligand stabilizes the HS state more than expected. The $\chi_M T$ product at room temperature is higher than the spin-only value of ∼3 cm^3 mol^{-1}K expected for $S = 2$ ($g = 2$), as often observed for HS Fe^{II} compounds. With the presence of small amounts of HS Fe^{III} (possibly resulting from oxidation of the prepared Fe^{II} materials) being discarded by their Mössbauer spectra (see following subsection), these high $\chi_M T$ values are attributed to the operation of spin−orbit coupling (SOC). The $^5T_2$ ground state is split by SOC, yielding levels separated by energies on the order of kT (thermally populated in the high-temperature range), which results in slightly temperature-dependent $\chi_M T$ values above ca. 60 K.[37]

Mössbauer Spectroscopy. The HS state of Fe^{II} in complexes **5** and **6** is confirmed by their Mössbauer spectra showing a unique quadrupole split doublet with parameters characteristic of HS Fe^{II} ($\delta = 1.151(4)$ and 1.118(4), and $\Delta E_Q = 2.478(8)$ and 2.258(7) mm s^{-1} at 80 K for **5** and **6**, respectively).

Crystal Structure of Complex 6. In the molecular structure of complex **6**, [FeL^{D4}(NCS)$_2$], the presence of the bulky and electron-attracting 6-bromo substituent on the pyridine moiety induces a strong deformation of the octahedral symmetry around Fe^{II}, as evidenced by the bond length and bond angle values reported in Table 3. The planar conformation of the ligand in this molecular structure is stabilized by an intramolecular C−H···Br bond (C1···Br1 = 3.434(3) Å and C1−H···Br1 = 128.8°), characteristic of this type of weak interaction.[38] This leads to the formation of a pseudomacrocycle around the iron(II) center, which further stabilizes the complex through a supplementary six-membered pseudometallacycle (Figure 13). The crystal structure of the HS complex **6** resembles that of complex **3** in the HS state at 350 and 400 K. It essentially results from the packing of similar centrosymmetric dinuclear {[FeL^{D4}(NCS)$_2$]}$_2$ units stabilized through $\pi-\pi$ interactions and two strong intermolecular H-bonds with distance N7···N6′ ($2 - x, 1 - y, 1 - z$) = 3.028(3) Å and angle N7−H···N6′ = 145.9°. Further extension of the structure into 2D layers occurs through weak C−H···S contacts.

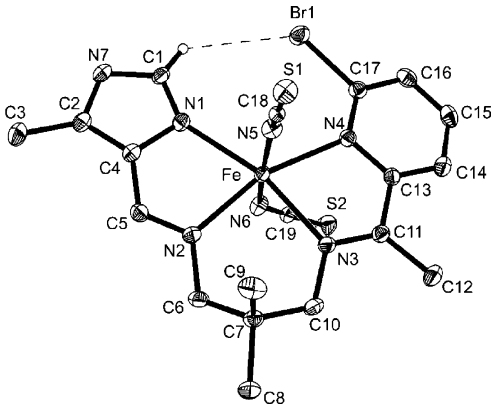

Figure 13. ORTEP view of complex **6**, [FeL^{D4}(NCS)$_2$]. For clarity, hydrogen atoms not involved in hydrogen interactions are omitted.

Table 3. Selected Bond Lengths (Å) and Bond Angles)deg) for [FeL^{D4}(NCS)$_2$], 6, at 180 K

Fe−N	length (Å)	N−Fe−N	angle (deg)
Fe−N1	2.245(2)	N1−Fe−N5	88.52(9)
Fe−N2	2.154.(2)	N2−Fe−N3	88.73(8)
Fe−N3	2.194(2)	N2−Fe−N4	162.90(8)
Fe−N4	2.247(2)	N2−Fe−N5	97.63(9)
Fe−N5	2.092(3)	N2−Fe−N6	90.55(9)
Fe−N6	2.199(2)	N5−Fe−N6	171.26(9)

Concluding Remarks

This work further explores SCO materials built from tetradentate ligands including exclusive nitrogen donors associated with coordinating pseudohalide anions. We have previously combined acetylpyridine and 2R-imidazole-4-carboxaldehyde (R═H, Me, Ph) as carbonyl synthons, and 1,3-diaminopropane and 2,2-dimethyl-1,3-diaminopropane as diamino synthons for preparing dissymmetrical L^{Cx} bis-Schiff bases chelated to Fe^{II} with trans-coordinated NCS$^-$ that have brought the ligand field onto Fe^{II} to the intermediate range suitable for SCO in the [FeL^{Cx}(NCS)$_2$] series.[6] Because the

(37) Mabbs, F. E.; Machin, D. J. *Magnetic and Transition Metal Complexes*; Chapman and Hall: London, 1973.

(38) (a) Steiner, T. *Angew. Chem., Int. Ed.* **2002**, *41*, 48. (b) Desiraju, G.; Steiner, T. *The Weak Hydrogen Bond in Structural Chemistry and Biology*; Oxford University Press: Oxford, 2001.

difference in SCO temperatures $T_{1/2}$ within the $[FeL^{Cx}(NCS)_2]$ series has previously evidenced the prominent electronic effect exerted by the 2-R imidazolyl substituent in tuning the ligand field onto Fe^{II}, in the present study we have kept 2-R imidazolyl = H, allowed the same R_1 substituents (H and Me), and considered the effect of (i) a 5-R imidazolyl ring substituent, Me, (ii) a pyridyl ring substituent, 6-Br, and, (iii) replacement of *trans*-NCS^- by *trans*-$NCSe^-$ ligands.

$[FeL^{D1}(NCS)_2]\cdot H_2O$ (**1**) and $[FeL^{D1}(NCSe)_2]\cdot H_2O$ (**2**) with R_1 = H, 5-R(imidazolyl) = Me, and NCS^- and $NCSe^-$ apical ligands (Chart 1), respectively, are LS up to ~350 K, where they start losing crystallization water. At 400 K, when all water has been removed, $[FeL^{D1}(NCS)_2]$ and $[FeL^{D1}(NCSe)_2]$ are 100 and ~60% HS, respectively, and show quite different SCO behaviors. Whereas $[FeL^{D1}(NCS)_2]$ exhibits a two-step SCO with a smooth low-temperature step centered at $T^{\downarrow}_{1/2} \approx 202$ K and a steep and hysteretic high-temperature step around room temperature ($T^{h}_{1/2}\downarrow = 292$ K and $T^{h}_{1/2}\uparrow = 303$ K), $[FeL^{D1}(NCSe)_2]$ exhibits a smooth one-step SCO centered at $T_{1/2} \approx 350$ K. Mössbauer spectroscopy clearly showed the presence of two LS doublets in the dehydrated form of **1** and **2** at low temperature, thus confirming the presence of two distinct LS Fe^{II} sites, whereas only one doublet with very broad components was observed for the HS phase. Also, only one LS site was observed for the corresponding hydrated species. As reported earlier,[39] the loss of water induces significant changes in the molecular structure, particularly in the hydrogen bond network.

$[FeL^{D2}(NCS)_2]$ (**3**) and $[FeL^{D2}(NCSe)_2]$ (**4**) with R_1 = 5-R(imidazolyl) = Me, and NCS^- and $NCSe^-$ apical ligands (Chart 1), respectively, are also LS at room temperature. **3** exhibits a very steep and hysteretic SCO around 315 K ($T_{1/2}\downarrow = 313$ K and $T_{1/2}\uparrow = 317$ K), whereas **4** exhibits the onset of SCO behavior above 350 K. The steep SCO of **3**, characterized by a 4 K wide hysteresis, is not associated with a crystallographic phase transition: both spin-state isomers crystallize in the same $P\bar{1}$ space group. However, the presence of hysteresis is evidence of the first-order SCO of **3**, which results most probably from the significant and reversible differences in the supramolecular structure of the LS and HS phases: NH···SCN short contacts, $\pi-\pi$ stackings of imidazolyl rings, and C−H···S and S···S contacts yield a 2D supramolecular structure of the LS phase, whereas NH···NCS short contacts, $\pi-\pi$ stackings of imidazolyl rings and S···S contacts yield a 1D supramolecular structure of the HS phase.[36]

It is also worth noticing that a statistical order−disorder rearrangement of the C6 to C10 fragment inside L^{D2} accompanies the thermal SCO for ~20% of the molecules. This type of phenomenon has been discussed in the SCO literature for a long time, but mostly in the case of the disorder of species not coordinated to Fe^{II}, i.e., counter anions[40] or solvent molecules.[41] For example, in the case of $[Fe(2\text{-pic})_3]Cl_2\cdot EtOH$, it has been considered that thermal ordering of the ethanol molecule hydrogen bonded to $[Fe(2\text{-pic})_3]^{2+}$ triggers the SCO.[41a,42] The order−disorder phenomenon has also been evidenced by Mössbauer spectroscopy, through the asymmetry induced in LS and HS lines.[40b,43] Recently, Matouzenko et al.[44] have described the first example of an SCO system with an order−disorder transition involving the ligand to Fe^{II}. $[Fe(DAPP)(abpt)](ClO_4)_2$, where DAPP = [bis(3-amino-propyl)(2-pyridylmethyl)amine] and abpt = 4-amino-3,5-bis(pyridin-2-yl)-1,2,4-triazole, exhibits a steep HS ↔ LS transition with a 10 K wide thermal hysteresis centered at 176 K and an order−disorder rearrangement inside the DAPP ligand. $[FeL^{D2}(NCS)_2]$ (**3**) is thus the second example of an SCO complex exhibiting this type of behavior: the asymmetry observed in the Mössbauer spectra may arise from relaxation between isomers of the complex corresponding to the two conformations of the tetradentate ligand. An investigation of the possible relationship between such a structural change and the magnetic properties of this material using DFT calculations is in progress.

The $NCSe^-$ vs NCS^- substitution yields dramatic effects on the SCO properties of materials **1**−**4**: it induces an increase in $T_{1/2}$ greater than 100 K for $[FeL^{D2}(NCSe)_2]$ (**4**) with respect to $[FeL^{D2}(NCS)_2]$ (**3**) and ~55 K for $[FeL^{D1}(NCSe)_2]$ (dehydrated **2**) with respect to $[FeL^{D1}(NCS)_2]$ (dehydrated **1**). In both cases, whereas the SCO is steep for the thiocyanate materials **1** (high-temperature step) and **3**, it is smooth for the selenocyanate ones, **2** and **4**, thus preventing observation of a two-step SCO in complex **2**, although two distinct Fe^{II} sites are present. These results are in line with similar observations interpreted as originating from both electronic and mass effects ($M_{Se}/M_S = 2.5$).[45] For a system of effective mass m_{eff} and force constant k, in the harmonic approximation, the vibration frequency is $\nu = (k/m_{eff})^{1/2}$; the

(39) Giménez-López, M. C.; Clemente-León, M.; Coronado, E.; Romero, F. M.; Shova, S.; Tuchagues, J.-P. *Eur. J. Inorg. Chem.* **2005**, 2783.

(40) (a) Fleisch, J.; Gütlich, P.; Hasselbach, K. M.; Müller, W. *Inorg. Chem.* **1976**, *15*, 958. (b) König, E.; Ritter, G.; Kulshreshtha, S. K.; Nelson, S. M. *Inorg. Chem.* **1982**, *21*, 3022. (c) Wiehl, E. *Acta Crystallogr., Sect. B* **1993**, *29*, 289. (d) Breuning, E.; Ruben, M.; Lehn, J.-M.; Renz, F.; Garcia, Y.; Ksenofontov, V.; Gütlich, P.; Wegelius, E.; Rissanen, K. *Angew. Chem., Int. Ed.* **2000**, *39*, 2504. (e) Holland, J. M.; McAllister, J. A.; Lu, Z.; Kilner, C. A.; Thornton-Pett, M.; Halcrow, M. A. *Chem. Commun.* **2001**, 577.

(41) (a) Mikami, M.; Konno, M.; Saito, Y. *Chem. Phys. Lett.* **1979**, *63*, 566. (b) Mikami, M.; Konno, M.; Saito, Y.; *Acta Crystallogr., Sect. B* **1980**, *36*, 275. (c) Katz, B. A.; Strouse, C. E. *J. Am. Chem. Soc.* **1979**, *101*, 6214. (d) König, E.; Ritter, G.; Kulshreshtha, S. K.; Waigel, J.; Sacconi, L. *Inorg. Chem.* **1984**, *23*, 1241. (e) Wiehl, L.; Kiel, G.; Köhler, C. P.; Spiering, H.; Gütlich, P. *Inorg. Chem.* **1986**, *25*, 1565. (f) Conti, A. J.; Chadha, R. K.; Sena, K. M.; Rheingold, A. L.; Hendrickson, D. N. *Inorg. Chem.* **1993**, *32*, 2670. (g) Conti, A. J.; Kaji, K.; Nagano, Y.; Sena, K. M.; Yumoto, Y.; Chadha, R. K.; Rheingold, A. L.; Sorai, M.; Hendrickson, D. N. *Inorg. Chem.* **1993**, *32*, 2681.

(42) Chernyshov, D.; Hostettler, M.; Törnroos, K. W.; Bürgi, H.-B. *Angew. Chem., Int. Ed.* **2003**, *42*, 3825.

(43) Poganiuch, P.; Descurtins, S.; Gütlich, P. *J. Am. Chem. Soc.* **1990**, *112*, 3270.

(44) Matouzenko, G. S.; Bousseksou, A.; Borshch, S. A.; Perrin, M.; Zein, S.; Salmon, L.; Molnar, G.; Lecocq, S. *Inorg. Chem.* **2004**, *43*, 227.

(45) (a) Baker, W. A.; Bobonisch, H. M. *Inorg. Chem.* **1964**, *3*, 1184. (b) Konig, E.; Madeja, K. *Chem. Commun.* **1966**, 61. (c) Real, J.-A.; Bolvin, H.; Bousseksou, A.; Dworkin, A.; Kahn, O.; Varret, F.; Zarembovitch, J. *J. Am. Chem. Soc.* **1992**, *114*, 4650. (d) Real, J.-A.; Castro, I.; Bousseksou, A.; Verdaguer, M.; Burriel, R.; Castro, M.; Linares, J.; Varret, F. *Inorg. Chem.* **1997**, *36*, 455. (e) Moliner, N.; Muñoz, M. C.; van Koningsbruggen, P. J.; Real, J.-A. *Inorg. Chim. Acta* **1998**, *274*, 1. (f) Moliner, N.; Muñoz, M. C.; Létard, S.; Létard, J.-F.; Solans, X.; Burriel, R.; Castro, M.; Kahn, O.; Real, J.-A. *Inorg. Chim. Acta* **1999**, *291*, 279. (g) Moliner, N.; Muñoz, M.; Létard, S.; Salmon, L.; Tuchagues, J.-P.; Bousseksou, A.; Real, J-A. *Inorg. Chem.* **2002**, *41*, 6997.

increase in $T_{1/2}$ upon $NCSe^-$ vs NCS^- substitution may be attributed to a ΔS decrease due to changes in the low-frequencies vibrations.

$[FeL^{D3}(NCS)_2]$ (**5**) and $[FeL^{D4}(NCS)_2]$ (**6**) with 5-R(imidazolyl) = Me, 6-R(pyridyl) = Br, NCS^- apical ligands, and R_1 = H and Me, respectively (Chart 1), are HS in the 80−300 K temperature range. Combination of the steric and electronic effects induced by the 6-bromo substituent on the pyridyl ring of the ligand stabilizes the HS state more than we expected. The bulky Br atom generates a strongly distorted coordination sphere around Fe^{II}, as shown by the structural study of **6**, which probably overpasses its electronic effects.

The NCS^- ($NCSe^-$) anions are trans-coordinated in compounds **1**−**6**, allowing us to consider the differences between the tetradentate ligands to be the sole origin of the different electronic behaviors among all materials considered not only in the present report but also in a previously studied series.[6] As estimated through $T_{1/2}$ values, the role of R_1 in tuning the ligand field may be described as an inductive effect: the lower $T_{1/2}$ is associated with R_1 = H vs Me (**1**, $T_{1/2}$ = 295 K vs **3**, $T_{1/2}$ = 315 K and **2**, $T_{1/2}$ = 350 K vs **4**, $T_{1/2}$ > 400 K), thus indicating that, indeed, the inductive effect of R_1 slightly lowers the ligand field with regard to its counterpart in each pair.

Acknowledgment. Financial support from the French Ministry for Education, Research, and Technology (doctoral grant to N.B.) and from the CNRS-DFG collaborative programme (postdoctoral grant to S.S.) is gratefully acknowledged. S. Bonhommeau and J.−F. Meunier (LCC) are acknowledged for carrying out numerical simulations and thermal analyses, respectively. J. Sanchez Costa (ICMCB) is acknowledged for carrying out the LIESST measurement of **3**. M. Sorai and G. J. Long are acknowledged for helpful discussions on calorimetric measurements and Mössbauer spectroscopy.

Supporting Information Available: X-ray crystallographic information files (CIF); Table SI.1 collating Mössbauer data for compounds **1**−**6** in PDF format. This material is available free of charge via the Internet at http://pubs.acs.org.

CM061524M